Journal of the Taiwan Institute of Chemical Engineers 72 (2017) 104–115

Contents lists available at ScienceDirect

Journal of the Taiwan Institute of Chemical Engineers

journal homepage: www.elsevier.com/locate/jtice

Phase-change heat transfer in a cavity heated from below: The effect of utilizing single or hybrid nanoparticles as additives

M. Ghalambaz[a,*], A. Doostani[a], E. Izadpanahi[b], A.J. Chamkha[c,d]

[a] Department of Mechanical Engineering, Dezful Branch, Islamic Azad University, Dezful, Iran
[b] Department of Mechanical and Materials Engineering, Florida International University, Miami FL 33174, United States
[c] Mechanical Engineering Department, Prince Mohammad Bin Fahd University, Al-Khobar 31952, Saudi Arabia
[d] Prince Sultan Endowment for Energy and Environment, Prince Mohammad Bin Fahd University, Al-Khobar 31952, Saudi Arabia

ARTICLE INFO

Article history:
Received 8 August 2016
Revised 31 December 2016
Accepted 18 January 2017
Available online 7 February 2017

Keywords:
Hybrid nanofluid
Nano-composite
Phase change heat transfer
Finite element method

ABSTRACT

The present study deals with the effects of hybrid nanoparticles on the melting process of a nano-enhanced phase-change material (NEPCM) inside an enclosure. The bottom side of the cavity is isothermal at a hot temperature while the top wall is isothermal at a cold temperature and the left and right walls are insulated. The governing partial differential equations are first non-dimensional form and then solved using the Galerkin finite element method. Some of the dimensionless parameters are kept constant such as the Prandtl number, the Rayleigh number, the Stefan number and the ratio between the thermal diffusivity of the solid and liquid phases while the volume fraction of nanoparticles, the conductivity and viscosity parameters, and the Fourier number are altered. It is found out that increasing the values of the nanoparticles volume fraction, viscosity and conductivity parameters leads to significant variations in the solid-liquid interface for large values of Fourier number. Moreover, increasing the conductivity parameter and decreasing the viscosity parameter at the same time can cause an augmentation in the liquid fraction.

1. Introduction

Latent heat thermal energy storage is an effective and reliable way of storing energy compared to the other ways of energy storage including thermochemical reactions. Thus, phase-change processes such as melting can play a vital role in today's need for energy storage. A small volume of Phase Change Materials (PCM) can store a significant amount of energy during a solid to liquid phase-change process. Nowadays, PCM are extensively utilized in a variety of application such as solar heating systems [2,38], cooling the electronic devices [15,26], finned heat pipe-assisted thermal energy storage systems [44,45] and waste heat recovery [31,32,35]. Unfortunately, PCM employed in energy storage units have low thermal conductivity which reduce the heat absorption rate. Several methods are proposed to increase the thermal performance of the storage units, among them, using nanoparticles can enhance the thermal conductivity of a PCM even for a small volume fraction of nanoparticles.

A comprehensive study has been done regarding the effects of nanoparticles on the enhancement of the thermophysical and heat transfer potential of the conventional fluids. Rashidi et al. [36] have studied the thermal behavior of Al_2O_3–water and γ Al_2O_3–$C_2H_6O_2$ nanofluids in boundary layer over a vertical stretching sheet. They reported that both of the dynamic viscosity and thermal conductivity of the investigated nanofluids can significantly affect the thermal behavior of nanofluids. Ismael et al. [19] and Chamkha et al. [7] addressed the natural convective heat transfer of copper-water nanofluids in cavities. They concluded that the presence of nanoparticles could enhance the heat transfer; however, the heat transfer enhancement of nanofluids is under the significant influence of the flow conditions. Makulati et al. [29] have addressed the natural convective heat transfer of Al_2O_3-water nanofluids in a C shape cavity. They studied the effect of nanoparticles volume fraction on the natural convective heat transfer and found that in some cases the presence of nanoparticles could decrease the heat transfer in the cavity. Sheremet et al. [40] have studied the effect of nanoparticles on the convective heat transfer of nanofluids in a porous medium. They found that the presence of nanoparticles in the porous media may suppress some of the natural convective heat transfer mechanisms. In another study Sheremet et al. [39] have analyzed the natural convective heat transfer of nanofluids in a cavity containing a hot solid block. The results show

* Corresponding author.
E-mail addresses: m.ghalambaz@iaud.ac.ir, m.ghalambaz@gmail.com (M. Ghalambaz), doostaniali@gmail.com (A. Doostani), eizad001@fiu.edu (E. Izadpanahi), achamkha@pmu.edu.sa (A.J. Chamkha).

http://dx.doi.org/10.1016/j.jtice.2017.01.010
1876-1070/

Nomenclature

A_{mush}	mushy-zone constant (Carman–Koseny equation constant)
C_p	specific heat in constant pressure ($J/kg\,K$)
Fo	non-dimensional time
g	gravity (m/s^2)
H	length and height (m)
k	thermal conductivity ($W/m\,K$)
L	latent heat of fusion (J/kg)
Nc	conductivity parameter
$N\nu$	viscosity parameter
P	pressure (Pa)
Pr	Prandtl number
Ra	Rayleigh number
S	enclosure inclination angle
$S(T)$	Carman–Kozeny equation (source term)
Ste	Stefan number
t	time (s)
T	temperature (K)
T_f	melting temperature (K)
u	velocity in the x-direction (m/s)
$\boldsymbol{u}$	velocity vector (m/s)
v	velocity in the y-direction (m/s)
x,y	Cartesian coordinates

Greek symbols

(T)φ	liquid fraction
α	thermal diffiusivity (m^2/s)
ϕ	Volume fraction of nanoparticles
μ	dynamic viscosity (kg/m s)
ρ	density (kg/m^3)
ε	Carman–Kozeny equation constant
υ	kinematic viscosity (m^2/s)
$_{T\Delta}$	mushy-zone temperature range (K)
ξ	basis functions
$_{\gamma}$	the ratio of thermal diffiusivity
β	thermal expansion coefficient (1/K)
θ	on-dimensional temperature

Subscripts

bf	base fluid
c	cold
F	fusion
h	hot
hnf	hybrid nanofluid
i	interface position
k	node number
l	liquid phase
nf	nanofluid
p	particles
s	solid phase

the enhancement of heat transfer in the presence of nanoparticles. Additionally, phase change phenomena in nanofluids have been addressed by different researchers. Malvandi et al. [30] studied the film-wise condensation of nanofluids over a vertical plate. In order to modify the cooling rate, the thermophysical properties of nanofluids are subjected to change, and also the flow and heat and mass transfer are controlled throughout the domain. It is found that increasing nanoparticles volume fraction and normal temperature difference enhance the heat transfer rate, and it is also reported that the alumina nanoparticles offer better cooling performance compared to titania. In another attempt, the anisotropic behavior of magnetic nanofluids in film-wise condensation is investigated by Heysiattalab et al. [18] over a vertical plate. In this study, the modified Buongiorno model is used to observe the effects of nanoparticles slip velocity relative to the base fluid. It is reported that the heat transfer rate enhances when the magnetic field is aligned in the direction of the temperature gradient.

An augmentation in the thermal conductivity of a composite PCM has been reported by Zeng et al. [49] by using Ag nanoparticles. Liu et al. [27] reported a significant enhancement in the thermal conductivity of a PCM by suspending a small amount of TiO_2 nanoparticles in saturated $BaCl_2$. The effects of different nanoparticles such as Cu, Al, and C/Cu on the heat transfer rate of paraffin as a nano-enhanced phase-change material (NEPCM) have been investigated by Wu et al. [47]. They found that the heating and cooling times decreased by 30.3% and 28.2%, respectively, using a 1% Cu nanoparticles. Harikrishnan and Kalaiselvam [17] studied the solidification and melting time for the different volume fractions of CuO in an oleic phase-change material. They reported up to 27.67% and 28.57% reduction in solidification and melting times, respectively. These investigations have been done using single metallic or non-metallic nanoparticles. The non-metallic particles such as Al_2O_3 have an excellent stability and chemical inertness, although, they have lower thermal conductivities compared to the metallic nanoparticles.

Incorporation of a small amount of metal particles with non-metallic particles can outstandingly enhance the thermal properties. A copper–alumina composite briquette has been prepared by Jena et al. [20] from a homogeneous mixture of finely divided CuO and Al_2O_3 using the hydrogen reduction technique. The results reported by Suresh et al. [42] indicate that the augmentation in the viscosity is considerably higher than the increase in the thermal conductivity. A maximum enhancement of 13.56% in the Nusselt number has been reported by Suresh et al. [43] for Al_2O_3–Cu hybrid nanofluid. Esfe et al. [12] investigated the effect of nanoparticles volume fraction on the thermal conductivity and the dynamic viscosity. They utilized Ag–MgO/water hybrid nanofluid with nanoparticles volume fraction range between 0% and 2%, and then examined the accuracy of different existing theoretical and empirical correlations in predicting the value of the thermal conductivity and dynamic viscosity by comparing the predicted values with experimental data. Moghadassi et al. [33] numerically studied the effects of water-based Al_2O_3 and Al_2O_3–Cu hybrid nanofluid with a 0.1% volume concentration on laminar forced convective heat transfer. Their results revealed a much higher convective heat transfer coefficient for the hybrid nanofluid.

In view of the importance of phase-change materials and the beneficial characteristics of hybrid nanoparticles, the aim of the present research is to analyze the effect of a hybrid nanofluid on natural convection inside an enclosure which is filled with nano-enhanced phase-change material. The present study aims to answer the following questions regarding to phase change heat transfer of single/hybrid nanofluids:

I Does the presence of nanoparticles enhance the melting rate?
II From the literature review, it is clear that the presence of nanoparticles enhances the thermal conductivity and the dynamic viscosity of the NEPCM. The increase of the thermal conductivity tends to increase the heat transfer and the melting rate. In contrast, the increase of the dynamic viscosity tends to suppress the natural convective heat transfer. How does these two properties simultaneously affect the melting process of a NEPCM?
III What is the effect of the increase of the volume fraction of solid nanoparticles on the melting rate?

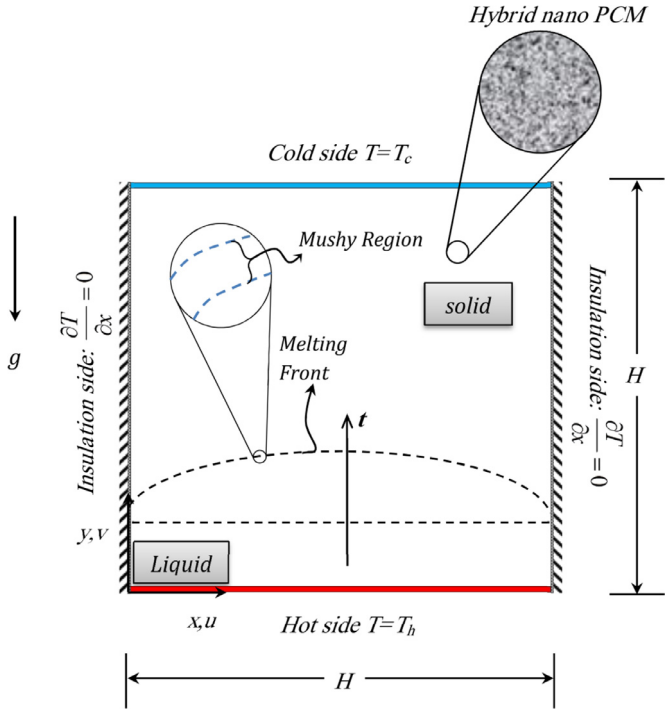

Fig. 1. A schematic for the physical model and geometry details.

2. Geometric and mathematical models

2.1. Physics of the problem

Consider a square cavity of size H (height and length H) which is filled with nano-enhanced phase-change material including hybrid nanoparticles. The bottom side of the enclosure is isothermal at a hot temperature T_h and the top wall is isothermal at a cold temperature T_c while the left and right walls are insulated. The coordinate system and the physical model of the cavity are shown in Fig. 1.

2.2. Governing equations

According to the physical model of the cavity, the governing partial differential equations can be written as follows [6,45]:

Continuity

$$\nabla \cdot \boldsymbol{u} = 0 \tag{1}$$

Momentum

$$\frac{\partial \vec{\boldsymbol{u}}}{\partial t} + (\boldsymbol{u}\cdot\nabla)\boldsymbol{u} = -\frac{1}{\rho_{hnf}}\nabla P + \frac{\mu_{hnf}}{\rho_{hnf}}\nabla\cdot(\mu(\varphi)\nabla\mathbf{u}) + \frac{\beta_{hnf}}{\rho_{hnf}}g\left(T-T_f\right) + \frac{1}{\rho_{hnf}}S(T)\boldsymbol{u} \tag{2}$$

Energy

$$\frac{\partial T}{\partial t} + \boldsymbol{u}\cdot\nabla T = \alpha_{hnf}\nabla(\alpha(\varphi)\nabla T) - \frac{L}{(C_p)_{hnf}}\frac{\partial\varphi(T)}{\partial t}. \tag{3}$$

It is worth noticing that in the writing of the above equations, the terms of viscosity related to ∇u^T have been neglected due to the fact that the variable dynamic viscosity is only utilized to assist the nanofluid velocity to smoothly reach the zero velocity in the solid part. The above equations in expanded form are as follows:

Continuity

$$\frac{\partial u}{\partial x} + \frac{\partial v}{\partial y} = 0 \tag{4}$$

Momentum in x-direction

$$\rho_{hnf}\left(\frac{\partial u}{\partial t} + u\frac{\partial u}{\partial x} + v\frac{\partial u}{\partial y}\right) = -\frac{\partial P}{\partial x} + \left(\frac{\partial}{\partial x}\left(\mu_{hnf}(\varphi)\frac{\partial u}{\partial x}\right) + \frac{\partial}{\partial y}\left(\mu_{hnf}(\varphi)\frac{\partial u}{\partial y}\right)\right) + S(T)u \tag{5}$$

Momentum in y-direction

$$\rho_{hnf}\left(\frac{\partial v}{\partial t} + u\frac{\partial v}{\partial x} + v\frac{\partial v}{\partial y}\right) = -\frac{\partial P}{\partial y} + \left(\frac{\partial}{\partial x}\left(\mu_{hnf}(\varphi)\frac{\partial v}{\partial x}\right) + \frac{\partial}{\partial y}\left(\mu_{hnf}(\varphi)\frac{\partial v}{\partial y}\right)\right) + \rho_{hnf}g\beta\left(T-T_f\right) + S(T)v \tag{6}$$

Energy

$$\left(\frac{\partial T}{\partial t} + u\frac{\partial T}{\partial x} + v\frac{\partial T}{\partial y}\right) = -\frac{1}{(\rho C_P)_{hnf}} + \left(\frac{\partial}{\partial x}\left(k_{hnf}\alpha(\varphi)\frac{\partial T}{\partial x}\right) + \frac{\partial}{\partial y}\left(k_{hnf}\alpha(\varphi)\frac{\partial T}{\partial y}\right)\right) + \frac{L}{(C_P)_{hnf}}\frac{\partial\varphi(T)}{\partial t} \tag{7}$$

Here $\alpha = \alpha_{l,\ hnf}\,\varphi + \alpha_{s,\ hnf}\,(1\text{-}\varphi)$ and φ is the melt fraction and can be evaluated using the temperature as follows:

$$\varphi(T) = \begin{cases} 0 & T < T_f \\ \frac{T-T_f}{\Delta T} & T_f < T < T_f + \frac{\Delta T}{2} \\ 1 & T > T_f + \Delta T \end{cases} \tag{8}$$

where ΔT is the mushy-zone temperature range, and also the viscosity is controlled in the mushy region utilizing the following relation:

$$\mu(\varphi) = \mu_l(1 + A_{mush}(1-\varphi)) \tag{9}$$

Controlling the viscosity according to Eq. (9) in the mushy region causes the velocity and the pressure fields to be uniform in the domain of the solution. In addition, it helps the velocity field to remain zero in the vicinity of the solid parts of the domain. The thermal diffusivity in the liquid, solid and mushy regions is a linear function of the volume fraction of the liquid as: $\alpha(\varphi)=\alpha_{l,\ hnf}\varphi+\alpha_{s,\ hnf}\,(1\text{-}\varphi)$.

In the momentum equation, the source term $S(T)$ is assumed as a continuous equation for phase transient exploiting the Carman–Kozeny equation as [3]:

$$S(T) = -A_{mush}\frac{(1-\varphi(T))^2}{\varphi(T)^3 + \varepsilon} \tag{10}$$

The buoyant force which causes the liquid phase to rise and natural convection happens, is modeled through the Boussinesq approximation as follows:

$$\vec{F} = \rho_{hnf}\beta\vec{g}\left(T-T_f\right) \tag{11}$$

Based on the problem description, the boundary conditions are given by:

$$\text{Heatedwall} \quad y=0: \quad u=0, \quad v=0, \quad T=T_h \tag{12a}$$

$$\text{Cooledwall} \quad y=H: \quad u=0, \quad v=0, \quad T=T_c \tag{12b}$$

$$\text{Leftwall} \quad x=0: \quad u=0, \quad v=0, \quad \frac{\partial T}{\partial x}=0 \tag{12c}$$

$$\text{Rightwall} \quad x=H: \quad u=0, \quad v=0, \quad \frac{\partial T}{\partial x}=0 \tag{12d}$$

where H is the width and height of the square enclosure.

The following dimensionless variables are introduced to change Eqs. (4)–(7) into the non-dimensional form.

$$X=\frac{x}{H}, Y=\frac{y}{H}, U=\frac{uH}{\alpha_{l,bf}}, V=\frac{vH}{\alpha_{l,bf}}, \theta=\frac{T-T_f}{T_h-T_f}, \tag{13a}$$

$$Fo=\frac{t\alpha_{bf}}{H^2}, S(\theta)=\frac{s(T)H^2}{\rho_{l,hnf}\alpha_{l,bf}}, \mu_r=\frac{\mu_{hnf}(\varphi)}{\mu_{bf}}, \quad \alpha_r=\frac{\alpha_{hnf}(\varphi)}{\alpha_{bf}}, P=\frac{PH^2}{\rho_{l,bf}\alpha_{l,bf}^2} \tag{13b}$$

Accordingly, the dimensionless parameters are obtained as follows:

$$Ra=\frac{g\beta_{bf}\left(T_h-T_f\right)L^3}{\alpha_{l,bf}\upsilon_{bf}}, Ste=\frac{C_{l,bf}\left(T_h-T_f\right)}{L}, Pr=\frac{\upsilon_{bf}}{\alpha_{l,bf}} \tag{14}$$

where *Ra*, *Ste*, and *Pr* are the Rayleigh number, the Stefan number, and the Prandtl number, respectively. Substituting Eqs. (13) and (14) into Eqs. (4)–(7), the non-dimensional form of the governing Eqs. (15)–(18) is obtained as follows:

Continuity:

$$\frac{\partial U}{\partial X}+\frac{\partial V}{\partial Y}=0 \tag{15}$$

Momentum in *X*-direction:

$$\frac{\partial U}{\partial Fo}+U\frac{\partial U}{\partial X}+V\frac{\partial U}{\partial Y} = -\frac{\rho_{bf}}{\rho_{hnf}}\frac{\partial P}{\partial X}+\frac{\rho_{bf}}{\rho_{hnf}}\frac{\mu_{hnf}}{\mu_{bf}}Pr\left(\frac{\partial}{\partial X}\left(\mu_r\frac{\partial U}{\partial X}\right)+\frac{\partial}{\partial Y}\left(\mu_r\frac{\partial U}{\partial Y}\right)\right) +\frac{\rho_{bf}}{\rho_{hnf}}S(\theta)U \tag{16}$$

Momentum in *Y*-direction:

$$\frac{\partial V}{\partial Fo}+U\frac{\partial V}{\partial X}+V\frac{\partial V}{\partial Y} = -\frac{\rho_{bf}}{\rho_{hnf}}\frac{\partial P}{\partial Y}+\frac{\rho_{bf}}{\rho_{hnf}}\frac{\mu_{hnf}}{\mu_{bf}}Pr\left(\frac{\partial}{\partial X}\left(\mu_r\frac{\partial V}{\partial X}\right)+\frac{\partial}{\partial Y}\left(\mu_r\frac{\partial V}{\partial Y}\right)\right) +\frac{\rho_{bf}}{\rho_{hnf}}S(\theta)V+PrRa\theta\frac{(\rho\beta)_{hnf}}{\rho_{hnf}\beta_{bf}} \tag{17}$$

Energy:

$$\frac{\partial \theta}{\partial Fo}+U\frac{\partial \theta}{\partial X}+V\frac{\partial \theta}{\partial Y} = \frac{\alpha_{hnf}}{\alpha_{bf}}\left(\frac{\partial}{\partial X}\left(\alpha_r\frac{\partial \theta}{\partial X}\right)+\frac{\partial}{\partial Y}\left(\alpha_r\frac{\partial \theta}{\partial Y}\right)\right) -\frac{(C_p)_{bf}}{(C_p)_{hnf}}\frac{1}{Ste}\frac{\partial \varphi(\theta)}{\partial Fo} \tag{18}$$

The thermal diffusivity ratio in energy equation can be evaluated as $\frac{\alpha_{hnf}(\varphi)}{\alpha_{l,bf}}=\frac{\varphi\alpha_{l,hnf}+(1-\varphi)\alpha_{s,hnf}}{\alpha_{l,bf}}$ which it can be rewritten as $\frac{\alpha_{hnf}(\varphi)}{\alpha_{l,bf}}=\varphi\alpha r_l+(1-\varphi)\alpha r_s$ where $\alpha r_l=\frac{\alpha_{l,hnf}}{\alpha_{l,bf}}$ and $\alpha r_s=\frac{\alpha_{l,hnf}}{\alpha_{l,bf}}$. Here, αr_l denotes the thermal diffusivity ratio of hybrid nanofluid and the base fluid for the liquid phase, and αr_s indicates the thermal diffusivity ratio of the hybrid nanofluid in the solid phase and the thermal diffusivity of the base fluid in the liquid phase. In the solid phase, the nanoparticles are trapped in the solid structure and they cannot freely move. In addition, as the volume fraction of the nanoparticles is very low, the changes in the thermophysical properties of the solid phase could be negligible. Hence, either it can be assumed that the thermal diffusivity of the solid hybrid nanofluid ($\alpha_{s,\,hnf}$) is equal to the thermal diffusivity of the solid base fluid ($\alpha_{s,\,bf}$), which as a result yields $\alpha_{s,\,bf}\,/\,\alpha_{l,\,bf}\approx 1$ or the thermal diffusivity of the solid hybrid nanofluid ($\alpha_{s,\,hnf}$) can be evaluated using the Maxwell model (Nc≈4.0) for nanofluids. It is worth considering that the change in the thermal diffusivity of the liquid hybrid nanofluid ($\alpha_{l,\,hnf}$) due to the presence of hybrid nanoparticles is quite significant, and it must be considered.

Eqs. (15)–(18) are subjected to the following boundary conditions. By using the variables (13), the non-dimensional boundary conditions become:

$$\text{Heatedwall} \quad Y=0: \quad U=0, \quad V=0, \quad \theta_h=1 \tag{19a}$$

$$\text{Coolingwall} \quad Y=AR: \quad U=0, \quad V=0, \quad \theta_c=0 \tag{19b}$$

$$\text{Leftwall} \quad X=0: \quad U=0, \quad V=0, \quad \frac{\partial \theta}{\partial x}=0 \tag{19c}$$

$$\text{Rightwall} \quad X=1: \quad U=0, \quad V=0, \quad \frac{\partial \theta}{\partial x}=0 \tag{19d}$$

where *U*, *V*, *C*, *P* and *T* are the *X*-velocity, *Y*-velocity, volume fraction of nanoparticles, pressure and the temperature of the nanofluid, respectively. The subscripts *hnf*, *bf* and *p* denote the nanofluid, the base fluid and the nanoparticles, respectively. The melt volume fraction as a function of θ is written as:

$$\varphi(T)=\begin{cases}0 & \theta<0\\ \frac{\theta}{\Delta\theta} & 0<\theta<\Delta\theta\\ 1 & \theta>\Delta\theta\end{cases} \tag{20}$$

Where $\Delta\theta=\frac{\Delta T}{T_h-T_f}$. The initial temperature in the non-dimensional form is evaluated as $\theta=0$ in the cavity. Following the study of Zaraki et al. [48], the dynamic viscosity ratio and the thermal conductivity ratio can be evaluated using:

$$\frac{\mu_{hnf}}{\mu_{bf}}=(1+Nv\times\phi) \tag{21}$$

$$\frac{k_{hnf}}{k_{bf}}=(1+Nc\times\phi) \tag{22}$$

and

$$\frac{\alpha_{hnf}}{\alpha_{bf}}=\frac{k_{hnf}}{k_{bf}}\frac{(\rho C_P)_{bf}}{(\rho C_P)_{hnf}} \tag{23}$$

where *Nv* and *Nc* are respectively the number of the dynamic viscosity and the number of the thermal conductivity as discussed by Zaraki et al. [48]. *Nv* and *Nc* generally could be functions of the size of nanoparticles, shape of nanoparticles, type of nanoparticles, type of the base fluid, and the method of preparation. However, as discussed in Zaraki et al. [48], each synthesized nanofluid could have a unique value of *Nv* and *Nc* Zaraki et al. [48] which could be evaluated using a linear curve fit of the experimental data. Table 1 shows some evaluated values of *Nc* and *Nv* evaluated using curve fitting of the available experimental data available in the literature.

Table 1
The evaluated of *Nc* and *Nv* for different samples of single and hybrid nanofluids.

Case	Refs.	Bas fluid	Temperature (T)	Type	*Size (nm)	Shape	Relative fraction	*Nc*	*Nv*
1*	[12]	Water	–	Ag	25	Irregular	0.5	20.3	6.26
				MgO	40	Irregular	0.5		
2*	[42]	Water	32	Al_2O_3	17	Spherical	0.9 (g)	9.2	33.29
				Cu	17	Spherical	0.1 (g)		
3*	[41]	Water	20	MWCNT	10–30 L = 0.5–500 μm	Cubic	0.74 (g)	82.59	122.34
				Fe_3O_4	13	Cubic	0.26 (g)		
		Water	40	MWCNT	OD = 10–3 L = 0.5–500 μm	Cubic	0.74 (g)	106.05	132.71
				Fe_3O_4	13	Cubic	0.26 (g)		
4*	[46]	EG	30	ZnO	35–45	Spherical	0.5	6.68	–
				TiO_2	30	Spherical	0.5		
		EG	40	ZnO	35–45	Spherical	0.5	8.82	–
				TiO_2	30	Spherical	0.5		
5*	[28]	Water	60	Cu	55	Spherical	0.5(g)	4.03	–
				TiO_2	55	Spherical	5(g)		
6*	[11]	SAE40	25	MWCNTs	OD = 5–15 ID = 3–5	–	0.2	–	38.62
				SiO_2	20–30	–	0.8		
		SAE40	30	MWCNTs	ID = 3–5 OD = 5–15	–	0.2	–	54.19
				SiO_2	20–30	–	0.8		
7*	[16]	EG	30	F-MWCNTs	ID = 3–5 OD = 5–15	–	0.5	10.45	–
				Fe_3O_4	20–30	Spherical	0.5		
		EG	40	F-MWCNTs	ID = 3–5 OD = 5–15	–	0.5	13.6	–
				Fe_3O_4	20–30	Spherical	0.5		
		EG	50	F-MWCNTs	ID = 3–5 OD = 5–15	–	0.5	18.11	–
				Fe_3O_4	20–30	Spherical	0.5		
8**	[34]	Eicosane	15	CuO	5–15	Spherical	–	1.31	–
		Eicosane	25	CuO	5–15	Spherical	–	1.20	–
		Eicosane	35	CuO	5–15	Spherical	–	4	–
9**	[34]	Eicosane	15	CuO	5–15	Spherical	–	1.76	–
		Eicosane	25	CuO	5–15	Spherical	–	2	–
		Eicosane	35	CuO	5–15	Spherical	–	3.58	–
10**	[34]	Eicosane	15	CuO	5–15	Spherical	–	1.23	–
		Eicosane	25	CuO	5–15	Spherical	–	1.57	–
		Eicosane	35	CuO	5–15	Spherical	–	2.14	–
11	[10]	Water	25	TiO_2	21	Spherical	–	3.87	7.65
12	[21]	Water	25	ZnO	150	Rectangular	–	3.86	13.20
13	[13]	Water	25	MgO	40	Spherical	–	7.70	12.05
14	[8]	Water	25	Al_2O_3	44	Spherical	–	14.1	15.62
15	[1]	Kerosene	25	Al_2O_3	21	Spherical	–	20.1	20.23

* Hybrid nanofluids;
** For the cases 8–10, each of the models are subject to different solidification procedures, *e.g.* ambient solidification, ice bath solidification and oven solidification method, respectively; ***OD: Out Diameter, *L*: Length, ID=Inner Diameter.

3. Method of solution and validation

First, the system of non-linear dimensionless partial differential Eqs. (15)–(18) and its boundary conditions (19) are transformed into a weak form, and then have been solved exploiting the Galerkin finite element method Zienkiewicz et al. [50]. The continuity equation (Eq. (15)) is used as a constraint to satisfy the mass conservation by control of the pressure distribution utilizing the mass conservation. Although, the following constraint equation for the continuity equation is utilized as a penalty parameter (χ) in the momentum equations as described by [37]. Therefore, the pressure can be written as

$$P = \chi\left(\frac{\partial U}{\partial X} + \frac{\partial V}{\partial Y}\right) \tag{24}$$

Here χ is the penalty number, which has a large value. Using Eq. (24), the momentum Eqs. (16) and (17) become as follows:

$$\begin{aligned}&\frac{\partial U}{\partial Fo} + U\frac{\partial U}{\partial X} + V\frac{\partial U}{\partial Y}\\ &= -\frac{\rho_{bf}}{\rho_{hnf}}\frac{\partial}{\partial X}\left(\chi\left(\frac{\partial U}{\partial X} + \frac{\partial V}{\partial Y}\right)\right)\\ &\quad + \frac{\rho_{bf}}{\rho_{hnf}}\frac{\mu_{hnf}}{\mu_{bf}}Pr\left(\frac{\partial}{\partial X}\left(\mu_r\frac{\partial U}{\partial X}\right) + \frac{\partial}{\partial Y}\left(\mu_r\frac{\partial U}{\partial Y}\right)\right)\\ &\quad + \frac{\rho_{bf}}{\rho_{hnf}}S(T)U\end{aligned} \tag{25}$$

$$\begin{aligned}&\frac{\partial V}{\partial Fo} + U\frac{\partial V}{\partial X} + V\frac{\partial V}{\partial Y}\\ &= -\frac{\rho_{bf}}{\rho_{hnf}}\frac{\partial}{\partial Y}\left(\chi\left(\frac{\partial U}{\partial X} + \frac{\partial V}{\partial Y}\right)\right)\\ &\quad + \frac{\rho_{bf}}{\rho_{hnf}}\frac{\mu_{hnf}}{\mu_{bf}}Pr\left(\frac{\partial}{\partial X}\left(\mu_r\frac{\partial V}{\partial X}\right) + \frac{\partial}{\partial Y}\left(\mu_r\frac{\partial V}{\partial Y}\right)\right)\\ &\quad + \frac{\rho_{bf}}{\rho_{hnf}}S(T)V + PrRa\theta\frac{(\rho\beta)_{hnf}}{\rho_{hnf}\beta_{bf}}\end{aligned} \tag{26}$$

In Eqs. (25) and (26), the continuity Eq. (15) is satisfied for very large values of the penalty parameter ($\chi = 10^7$) [37]. Now, the velocities (U and V) as well as the temperature, θ, are expanded calling a basis set $\{\xi_k\}_{k=1}^{N}$ in the domain interval of $-0.5 < X < 0.5$ and $0 < Y < 1$ as,

$$U \approx \sum_{k=1}^{N} U_k\xi(X,Y),\ V \approx \sum_{k=1}^{N} k_k\xi(X,Y),\ \theta \approx \sum_{k=1}^{N} \theta_k\xi(X,Y) \tag{27}$$

It is worth mentioning that the basis function ζ for all of the three variables are the same, thus, the total number of nodes is $N = 3$. By calling the introduced basis functions in Eq. (27), the nonlinear residual equations ($R^N{}_i$) of the governing equations,

Eqs. (15)–(18) can be rewritten as follows:

$$R_i^1 = \sum_{k=1}^{N} U_k \int_\Omega \frac{\partial \xi_k}{\partial Fo}\xi_i dXdY + \sum_{k=1}^{N} U_k \int_\Omega \left[\left(\sum_{k=1}^{N} U_k\xi_k\right)\frac{\partial \xi_k}{\partial X} + \left(\sum_{k=1}^{N} V_k\xi_k\right)\frac{\partial \xi_k}{\partial Y}\right]\xi_i dXdY + \frac{\rho_{bf}}{\rho_{hnf}}\left(\sum_{k=1}^{N} U_k \int_\Omega \frac{\partial \xi_i}{\partial X}\left[(\chi)\frac{\partial \xi_k}{\partial X}dXdY\right] + \sum_{k=1}^{N} V_k \int_\Omega \frac{\partial \xi_i}{\partial X}\left[(\chi)\frac{\partial \xi_k}{\partial Y}dXdY\right]\right) + \frac{\rho_{bf}}{\rho_{hnf}}\frac{\mu_{hnf}}{\rho_{bf}}Pr\left[\sum_{k=1}^{N} U_k \int_\Omega \frac{\partial \xi_i}{\partial X}\left(\mu_r \frac{\partial \xi_k}{\partial X}dXdY\right) + \sum_{k=1}^{N} U_k \int_\Omega \frac{\partial \xi_i}{\partial Y}\left(\mu_r \frac{\partial \xi_k}{\partial Y}dXdY\right)\right] + \frac{\rho_{bf}}{\rho_{hnf}}S(T)\sum_{k=1}^{N}\int_\Omega\left(\sum_{k=1}^{N}(U_k\xi_k)\xi_i\right)dXdY \quad (28)$$

$$R_i^2 = \sum_{k=1}^{N} V_k \int_\Omega \frac{\partial \xi_k}{\partial Fo}\xi_i dXdY + \sum_{k=1}^{N} V_k \int_\Omega \left[\left(\sum_{k=1}^{N} U_k\xi_k\right)\frac{\partial \xi_k}{\partial X} + \left(\sum_{k=1}^{N} V_k\xi_k\right)\frac{\partial \xi_k}{\partial Y}\right]\xi_i dXdY + \frac{\rho_{bf}}{\rho_{hnf}}\left(\sum_{k=1}^{N} U_k \int_\Omega \frac{\partial \xi_i}{\partial Y}\left[(\chi)\frac{\partial \xi_k}{\partial X}dXdY\right] + \sum_{k=1}^{N} V_k \int_\Omega \frac{\partial \xi_i}{\partial Y}\left[(\chi)\frac{\partial \xi_k}{\partial Y}dXdY\right]\right) + \frac{\rho_{bf}}{\rho_{hnf}}\frac{\mu_{hnf}}{\rho_{bf}}Pr\left[\sum_{k=1}^{N} V_k \int_\Omega \frac{\partial \xi_i}{\partial X}\left(\mu_r \frac{\partial \xi_k}{\partial X}dXdY\right) + \sum_{k=1}^{N} V_k \int_\Omega \frac{\partial \xi_i}{\partial Y}\left(\mu_r \frac{\partial \xi_k}{\partial Y}dXdY\right)\right] \quad (29)$$

$$R_i^3 = \sum_{k=1}^{N} \theta_k \int_\Omega \frac{\partial \xi_k}{\partial Fo}\xi_i dXdY + \sum_{k=1}^{N} \theta_k \int_\Omega \left[\left(\sum_{k=1}^{N} U_k\xi_k\right)\frac{\partial \xi_k}{\partial X} + \left(\sum_{k=1}^{N} V_k\xi_k\right)\frac{\partial \xi_k}{\partial Y}\right]\xi_i dXdY + \frac{\alpha_{bf}}{\alpha_{hnf}}\left(\sum_{k=1}^{N} \theta_k \int_\Omega \frac{\partial \xi_i}{\partial X}\left[\alpha_r \frac{\partial \xi_k}{\partial X}dXdY\right] + \sum_{k=1}^{N} \theta_k \int_\Omega \frac{\partial \xi_i}{\partial Y}\left[\alpha_r \frac{\partial \xi_k}{\partial Y}dXdY\right]\right) + \frac{(C_p)_{bf}}{(C_p)_{hnf}}\frac{1}{Ste}\sum_{k=1}^{N} f_k \int_\Omega \frac{\partial \xi_k}{\partial Fo}\xi_i dXdY \quad (30)$$

3.1. Grid check

The grid independency of the solution is examined by utilizing several grid sizes for the case of $Pr = 0.0216$, $Ra = 2.1 \times 10^5$, $Ste = 0.039$, $A_{mush} = 1.6 \times 10^6$ and $\phi = 0$ Table 2 presents the required time for simulation of approximately 90% of melting for various grid sizes. In order to study the phase-change process, a supercomputer with 40 GB of memory and 20 CPU cores each of 2.2 GHz is used. As seen, by the increase grid nodes, the required calculation time increases dramatically. Here, the variation of the liquid fraction versus different grid sizes is depicted in Fig. 2. The melting front (the interface of solid and liquid) is considered as $\varphi = 0.5$ in the present study. The results of this figure indicate that the grid size of 150×150 can provide accurate results for most of engineering applications and graphical illustration of the results in almost a reasonable time. Thus, in the present study the grid size 150×150 is used to carry out the results.

Table 2
The required time for grid size independency.

Cases	Grid size	Run time
Case 1	100×100	14 h, 21 min
Case 2	125×125	1 day, 6h, 12 min
Case 3	150×150	2 day, 1 h, 20 min
Case 4	175×175	2 days, 18 h, 27 mins
Case 5	200×200	3 days, 10 h, 48 min

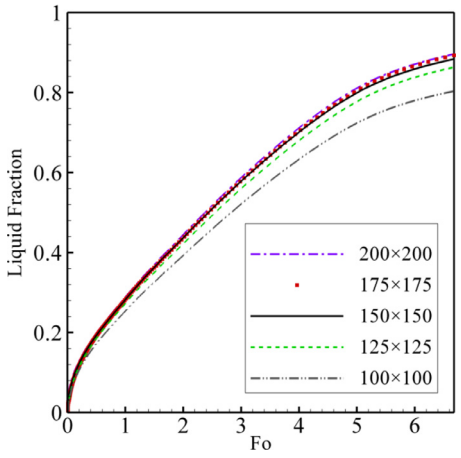

Fig. 2. The liquid fraction for various grid sizes.

3.2. Validation of the results

Several studies have been done to measure the accuracy of the present research. Firstly, the results of the present study are compared with both experimental Gau and Viskanta [14] and the numerical results available in the literature for the case of a rectangular cavity with an aspect ratio (height/width) of 0.714.

Gau and Viskanta [14] have examined the melting interface utilizing the pour-out method and the probing method. In their study, the left wall is hot while the top and bottom walls are insulated. Additionally, the evaluated melting interface for this problem is numerically reported by Kashani et al. [22], Khodadadi and Hosseinizadeh [23], Brent et al. [5] and Tiari et al. [44]. The summary of the available numerical results is plotted in Fig. 3. Clearly, the results of the present study are in acceptable agreement with the available results in the literature. In the case of $Fo = 3.48$, there is a difference between the present results and the experimental results, however, they show an acceptable agreement with the numerical results. In previous studies, the authors have concluded that the difference between the numerical and experimental results could be due to the method of evaluating the melting interface in the experiments of Gau and Viskanta [14], since they measured the melting interface mechanically exploiting a manual mechanical probe. In the case with high values of Fo, the solid-liquid

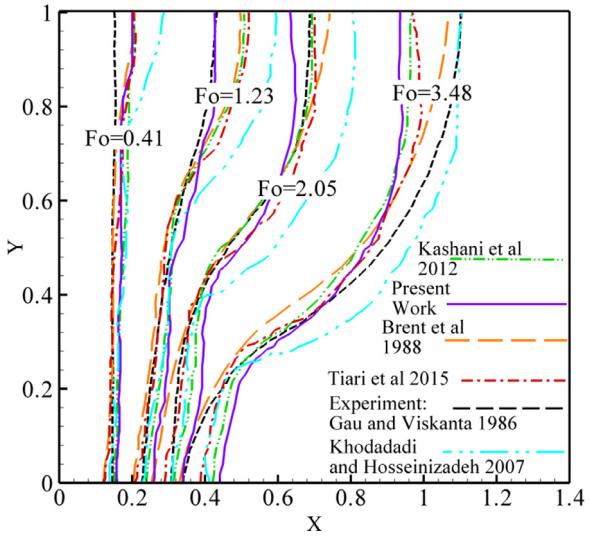

Fig. 3. A comparison of the experimental measurement of Gau and Viskanta [14] and numerical results available in literature with the results of the present study: isothermal hot wall at the left and isothermal cooled wall at the right while the bottom and top walls are insulated, $Ra = 6 \times 10^5$ $Pr = 0.0216$.

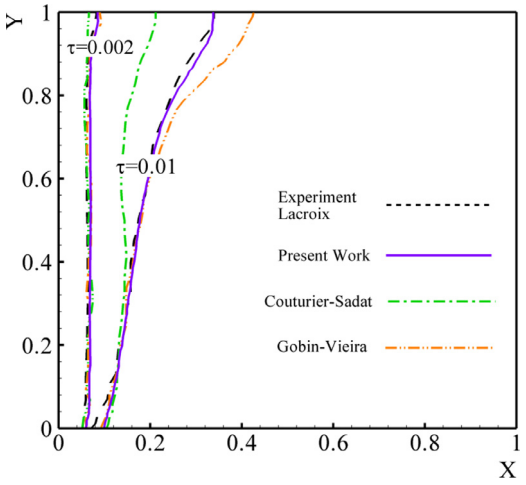

Fig. 4. A comparison of the benchmark study of Bertrand et al. [4] with the results of the present study ($\tau = Fo \times Ste$) when (a): (a): $\tau = 6 \times 10^{-3}$ (b): $\tau = 1 \times 10^{-2}$.

interface of melting could be unstable, as a result, distinguishing the exact shape of the interface is hard.

Secondly, a comparison is drawn between the results of the present finite element code and the benchmark study of Bertrand et al. [4] when $Ra = 1 \times 10^7$, Pr=50and $\alpha_s/\alpha_l = 1$, for which different authors have obtained the results of the melting interface for a square cavity. The results are depicted in Fig. 4. It can be seen that there is a good agreement between the results of the present study and the results available in the literature.

Finally, the results are compared with the experimental results reported by Kumar et al. [25] for melting of lead. Kumar et al. [25] have studied the melting of lead contained in a stainless steel cuboid, in which there was a heater located at one of the vertical side walls of the cavity, providing a constant heat flux, since

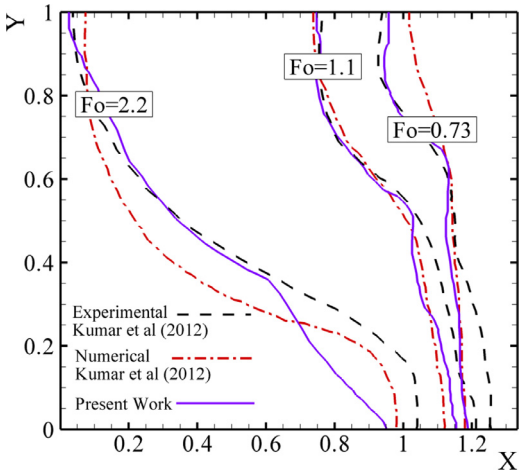

Fig. 5. The result of benchmark experimental of Kumar et al. [25] and the results of present study when $Fo = 0.37$, $Fo = 1.1$ and $Fo = 2.2$.

the other walls were insulated. The photography of the solid-liquid interface movement was carried out during melting of lead using neutron radiography. Table 3 presents the non-dimensional parameters of the experimental setup of Kumar et al. [25]. In the experiment of Kumar et al. [25], before melting started, the temperature was linearly distributed because the heater increased the temperature on both sides. However, after the melting started, the temperature at the right-hand side wall (the heater side) was higher than the left-hand side wall. Since the experiment by Kumar et al. [25] have been accomplished for the case of constant heat flux, the Rayleigh number, Stefan number and the Prandtl number should be calculated on the basis of the constant heat flux as $Ste^* = C_p q''_{cond} L^4_x/(kL)$ and the Rayleigh number based on constant heat flux can be written as $Ra^* = g\beta q''_{cond} L^4_y/(k\alpha\nu)$ and $Ste^* = C_p q''_{cond} L^4_x/(kL)$.

Fig. 5 depicts the comparison between the present results and the photography carried out by Kumar et al. [25] using neutron radiography. The solid-liquid interface has a curved shape in the present results and the results by Kumar et al. [25]. Additionally, both results show that the maximum and minimum depths occur at the top and bottom of the enclosure, respectively. Moreover, as Fo increases from 0.37 to 1.74, the depth of the solid-liquid interface increases which is accurately predicted by the present numerical results.

Finally, the results of the present study are compared with the results reported by Corcione [9] in Fig. 6 for the case of heating from bottom and cooling from top when $Pr = 0.71$ and $Ra = 10^6$. In Fig. 6, the streamlines and isotherms patterns of the present study are compared with the results of Corcione [9]. As it can be seen, the results are in a complete agreement with each other.

4. Results and discussion

An enclosure with the size of $L_x = 4.5$ cm, $L_y = 4.5$ cm filled with Octadecane is chosen for the model of the present study. The temperature at the bottom wall is T_h=40 ℃ and the temperature at the cold wall is T_c=30 ℃. The thermophysical properties of Octadecane are presented in Table 4. Accordingly, the

Table 3
Input provided for one case in simulation of Kumar et al. [25].

Heater input (right side)	Prandtl number	Stefan number	Rayleigh number	Temp at left side (K)	Temp at right side (K)
16.3 kW/m2	0.0236	0.4	1.4×10^7	555	599

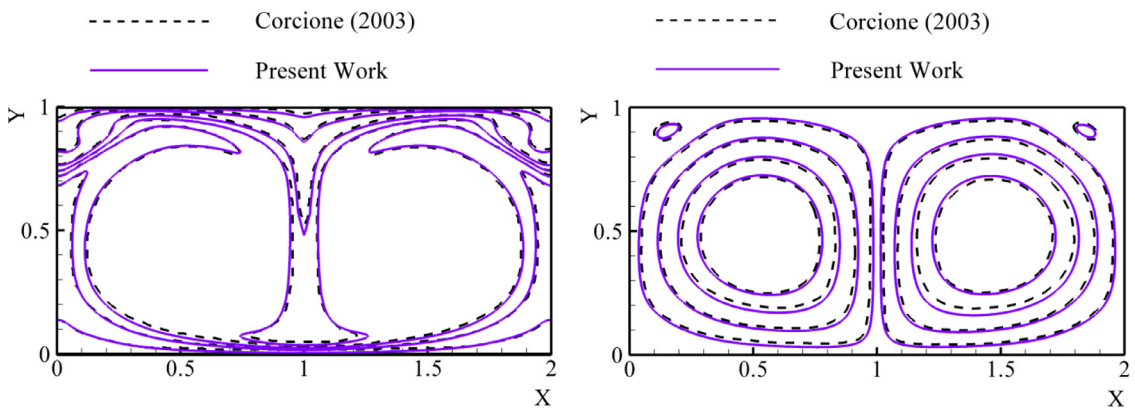

Fig. 6. The streamlines and isotherms patterns for $Ra = 10^6$, $Pr = 0.71$, A comparison of the study of Corcione [9] and the results of present study.

Table 4
Thermophysical properties of Octadecane.

Property	Symbol	Value	Unit
Density (Solid/Liquid)	ρ	800	(kg/m^3)
Thermal expansion coefficient	β	2×10^{-3}	$(1/K)$
Fusion temperature	T_f	303.16	(K)
Thermal conductivity (Solid/Liquid)	k	0.2	$(W/m\,K)$
Latent heat of fusion	L	1.25×10^{-5}	(J/kg)
Specific heat capacity (Solid/Liquid)	C	1250	$(J/kg\,K)$
Dynamic viscosity	μ	8×10^{-3}	$(kg/m\,s)$

corresponding non-dimensional parameters are: $Pr = 50$, $Ste = 0.1$, $Ra = 1 \times 10^7$ and $\alpha_s/\alpha_l = 1$. These non-dimensional parameters are considered as the default non-dimensional parameters in the present study. The calculations are carried out for this set of non-dimensional parameters otherwise the value of the non-dimensional parameter will be stated.

Following the experimental study of Esfe et al. [12] and theoretical study of Zaraki et al. [48], the magnitudes of ρ_{bf}/ρ_{hnf}, $(\rho C_p)_{bf}/(\rho C_p)_{hnf}$, C_{bf}/C_{hnf} and $\rho_{hnf}\beta_{bf}/(\rho\beta)_{hnf}$ for most of nanofluids is about unity. Indeed, by using nanoparticles in the base fluid only the thermal conductivity and dynamic viscosity of the resulting nanofluid would change dramatically. Therefore, by considering $(\rho C_p)_{bf}/(\rho C_p)_{hnf} \approx 1$ and using Eq. (22), the thermal diffusivity ratio α_{hnf}/α_{bf} can be simplified as

$$\frac{\alpha_{hnf}}{\alpha_{bf}} = \frac{k_{hnf}}{k_{bf}} \frac{(\rho C_P)_{bf}}{(\rho C_P)_{hnf}} = (1 + Nc \times \phi) \times (\approx 1) = 1 + Nc \times \phi \quad (31)$$

Thus, in the present study, ρ_{bf}/ρ_{hnf}, $(\rho C_p)_{bf}/(\rho C_p)_{hnf}$, C_{bf}/C_{hnf} and $\rho_{hnf}\beta_{bf}/(\rho\beta)_{hnf}$ are considered as unity. The dynamic viscosity ratio and the thermal conductivity ratio are evaluated using Eqs. (21) and (22); the thermal diffusivity ratio α_{hnf}/α_{bf} is also evaluated using Eq. (31).

Figs. 7–10 present the streamlines and isotherms for different values of the conductivity parameter, the viscosity parameter, the volume fraction of nanoparticles, and the Fourier number. As it is obvious, increasing the values of ϕ, Nc and Nv causes the depth of the solid-liquid interface to increase. Likewise, augmentation in the value of Fo leads to increasing the depth of the solid-liquid interface. Additionally, comparing the effects of the conductivity parameter, viscosity parameter and the volume fraction of nanoparticles for different values of Fourier number shows that for larger Fourier number, increasing ϕ, Nc and Nv has a much larger impact on the solid-liquid interface.

The effects of the nanoparticles volume fraction and the Fourier number on the melting front is depicted in Fig. 8, while the values of Nc and Nv are kept equal to 4 and 16, respectively. Obviously, increasing the volume fraction of nanoparticles from 0 to 2 significantly decreases the melting interface for large values of the Fourier number. In contrast, it is seen that increasing the nanoparticles volume fraction from 2 to 5 leads to a considerable augmentation in the melting interface depth. Comparing Fig. 8 with Figs. 9 and 10, illustrate the fact that the trend of changing the depth in the solid-liquid interface with the volume fraction of nanoparticles is not similar for different values of the conductivity and the viscosity parameters. For instance, in Fig. 10, in which the values of Nc and Nv are equal to 4 and 16, respectively, increasing the values of the nanoparticles volume fraction leads to the continuous development of the melting front for large values of the Fourier number.

Figs. 11–13 illustrate the effects of the conductivity and the viscosity parameters on the liquid fraction versus the Fourier number for different values of the nanoparticles volume fraction. Fig. 11 clearly shows that the liquid fraction significantly decreases as the conductivity parameter increases from 4 to 16, while the viscosity parameter is kept constant and equal to 16. Similarly, increasing the viscosity parameter from 4 to 16 causes a substantial decline in the values of the liquid fraction, as the conductivity parameter is equal to 16. The same trend can be observed in Fig. 13 in which the nanoparticles volume fraction is equal to 5%. However, in the case when ϕ is equal to 2% (Fig. 12), as the conductivity parameter increases from 4 to 16, the liquid fraction augments significantly. It is worth mentioning that in all the three cases it is predicted that when the conductivity parameter increases from 4 to 16 and at the same time the viscosity parameter decreases from 16 to 4, the liquid fraction increases, which means that the rate of the melting increases.

5. Conclusion

In the present study, the effects of the presence of nano additives on the natural convective melting process of nano-enhanced Octadecane inside a cavity are investigated. The governing set of equations was solved numerically using the Galerkin finite element method. The temperature at the bottom wall T_h is chosen to be higher than the fusion temperature. The Prandtl number, Rayleigh number, Stefan number and the ratio between the thermal diffusivity of the solid and liquid phases are kept constant equal to 50, 0.1, 1×10^7 and 1, respectively. The effects of several parameters such as the volume fraction of nanoparticles, the conductivity and viscosity parameters, and the Fourier number on the melting process caused by natural convection are reported. The results can be summarized as follows:

➢ The effects of the viscosity parameter, the conductivity parameter, and the volume fraction of nanoparticles for different values

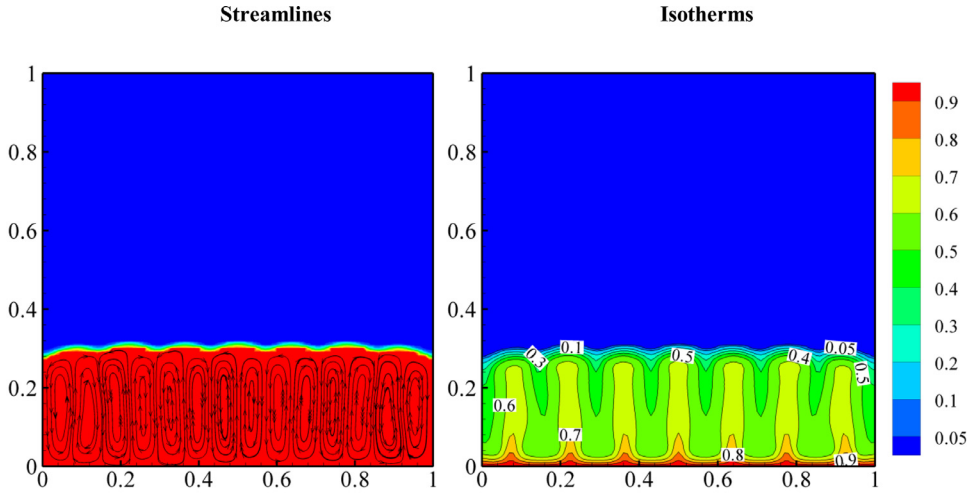

(a-1): ϕ=0%, Nc=Nv=0

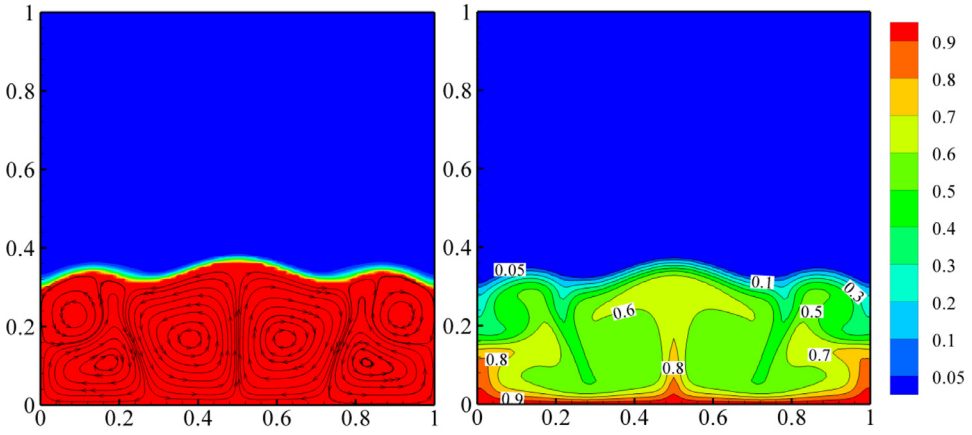

(a-2): ϕ=5%, Nc=16, Nv=4

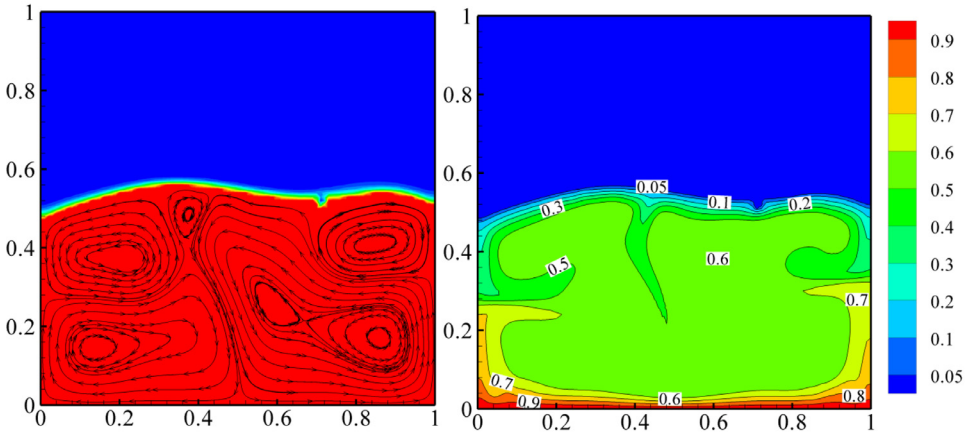

(b-1): ϕ=0%, Nc=Nv=0

Fig. 7. Streamlines and isotherms, when (a): $F_o = 0.15$ (b): $F_o = 0.35$ (c): $F_o = 0.6$.

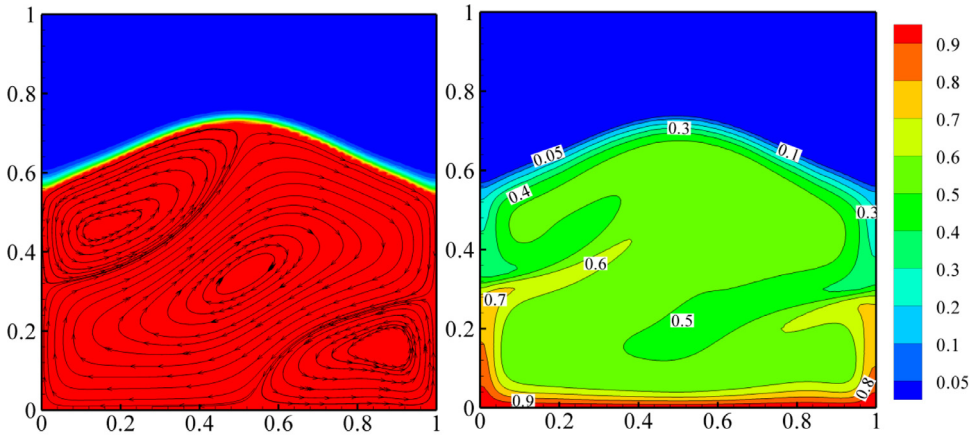

(b-2): ϕ=5%, Nc=16, Nv=4

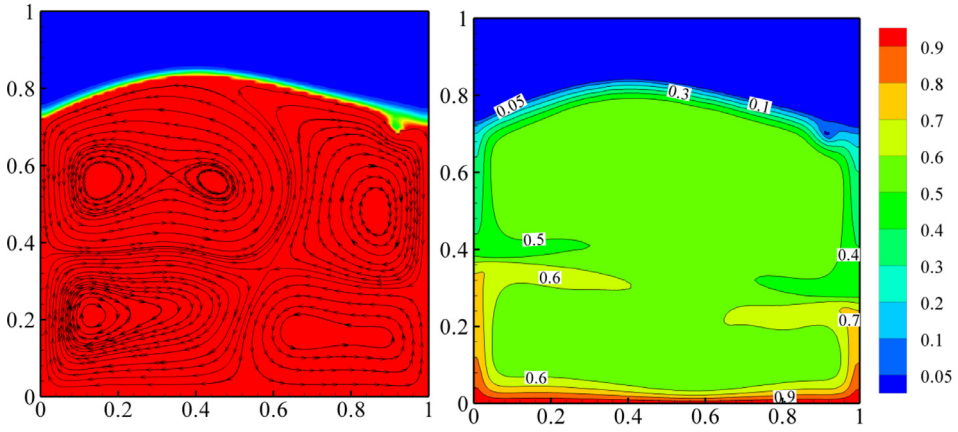

(c-2): ϕ=0%, Nc=Nv=0

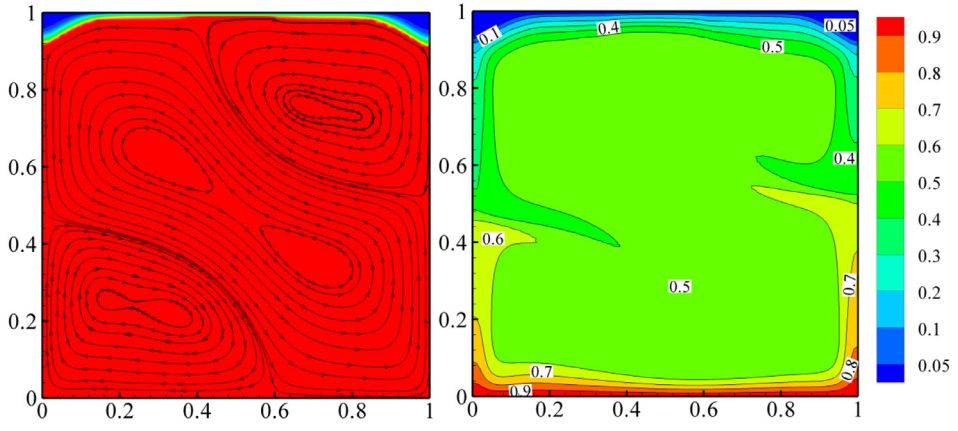

(c-2): ϕ=5%, Nc=16, Nv=4

Fig. 7. Continued

of the Fourier number indicate that for larger Fourier numbers, augmentation in ϕ, Nc and Nv causes larger variations in the solid-liquid interface.

➢ As the values of the nanoparticles volume fraction rise, continuous increases in the depth of the melting front for large values of the Fourier number can be observed, while the values of Nc and Nv are equal to 4 and 16, respectively.

➢ Increasing the conductivity parameter from 4 to 16 and simultaneously decreasing the viscosity parameter from 16 to 4 lead to increasing the rate of the melting of the solid phase.

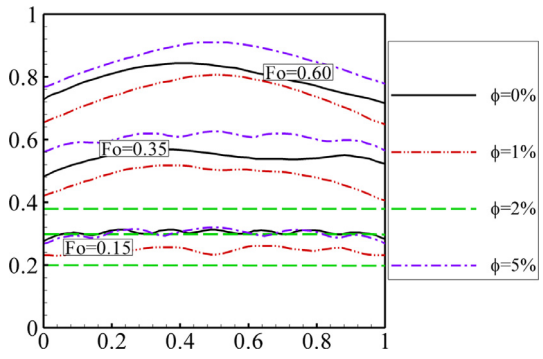

Fig. 8. The melting front for $Nc = 4$, $Nv = 16$.

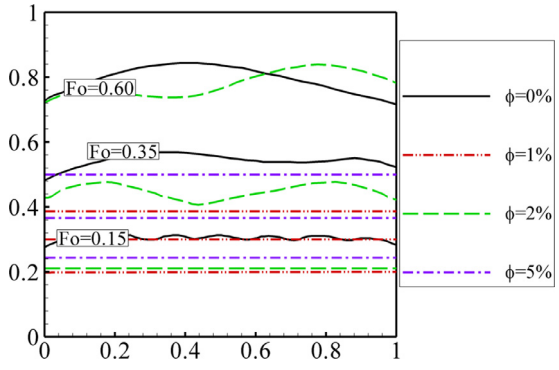

Fig. 9. The melting front for $Nc = 16$, $Nv = 16$.

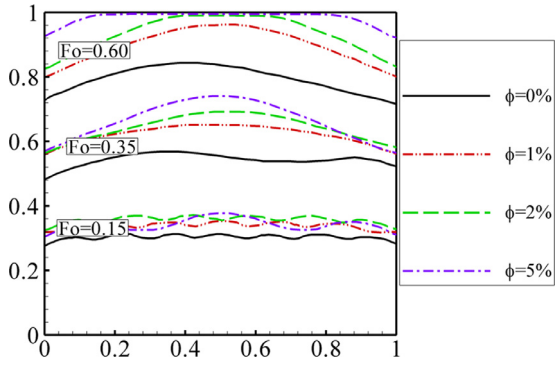

Fig. 10. The melting front for $Nc = 16$, $Nv = 4$.

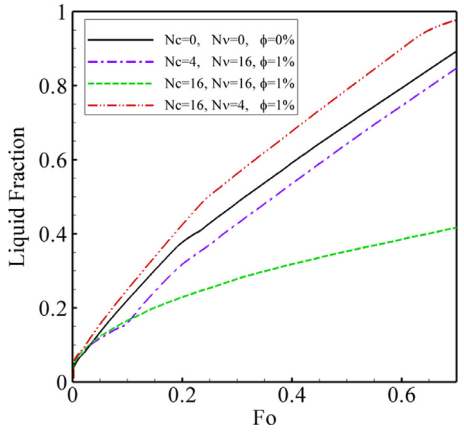

Fig. 11. Effect of $\phi = 1\%$ Volume fraction of nano-hybrid on liquid fraction for various Nc and Nv.

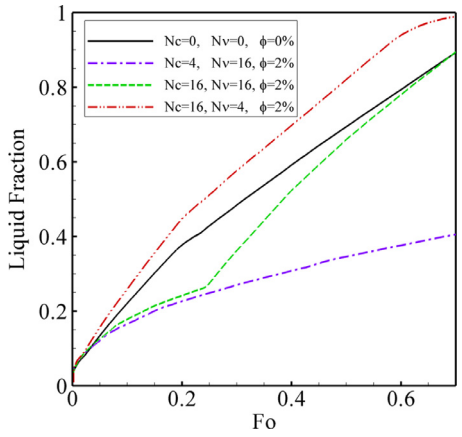

Fig. 12. Effect of $\phi = 2\%$ Volume fraction of nano-hybrid on liquid fraction for various Nc and Nv.

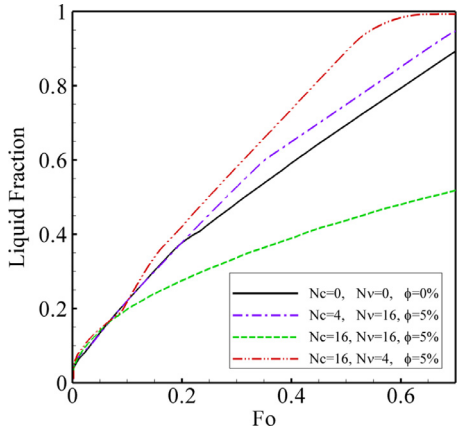

Fig. 13. Effect of $\phi = 5\%$ Volume fraction of nano-hybrid on liquid fraction for various Nc and Nv.

It is worth mentioning that the low thermal conductivity of a phase change material is the barrier for the efficiency of a thermal system in many applications. In a Latent Heat Storage (LHS) system, a PCM is commonly utilized in sealed packages. Each pack of PCM is subject to the heat transfer with the working flow. For example, in a solar energy system, the day light energy can be stored in the PCM and then utilized during the night hours. In addition, the release rate of the stored energy could be significantly higher than its storage rate due to different demands. However, the PCM packs can only absorb or release a limited amount of thermal energy at a time. The heat transfer potential of a PCM pack is limited by the effective surface area of the package and the heat conductivity or natural convection mechanism inside the package. Thus, any practical method for the increase of the thermal conductivity and heat transfer in a PCM package could be of great interest. As a result, a NEPCM with enhanced thermophysical properties can be a potential candidate to be utilized as an alternative phase change media to the regular phase change material. In this regard, in an invention, Khodadadi et al. [24] demonstrated that dispersed nanoparticles in the phase change material exhibit enhanced thermal conductivity in comparison to the base phase change material. In accordance with the results of the present study, the use of nanoparticles with a high thermal conductivity parameter (Nc) and a low dynamic viscosity parameter (Nv), finally improves the heat transfer rate of the thermal storage. However, there are other technological aspects such as the cost of nanoparticles and the overall amount of the heat storage and the entropy generation yet needed to be discussed in future studies.

Acknowledgements

This research is financially supported by Dezful Branch, Islamic Azad University, Dezful, Iran. The authors like to express their appreciation to Sheikh Bahaei National High-Performance Computing Center (SBNHPCC) for providing computational resources, supported by the scientific and technological department of the presidential office and Isfahan University of Technology (IUT). The authors are also thankful to Iran Nanotechnology Initiative Council (INIC) and National Iranian Drilling Company (NIDC) for the financial support of the present study.

References

[1] Agarwal DK, Vaidyanathan A, Kumar SS. Synthesis and characterization of kerosene–alumina nanofluids. Appl Therm Eng 2013;60:275–84.
[2] Agyenim F. The use of enhanced heat transfer phase change materials (PCM) to improve the coefficient of performance (COP) of solar powered LiBr/H_2O absorption cooling systems. Renew Energy 2016;87:229–39.
[3] Alpak FO, Lake LW, Embid SM. Validation of a modified Carman–Kozeny equation to model two-phase relative permeabilities. In: Proceedings of SPE Annual Technical Conference and Exhibition. Society of Petroleum Engineers; 1999.
[4] Bertrand O, Binet B, Combeau H, Couturier S, Delannoy Y, Gobin D, et al. Melting driven by natural convection A comparison exercise: first results. Int J Thermal Sci 1999;38:5–26.
[5] Brent A, Voller V, Reid KtJ. Enthalpy-porosity technique for modeling convection-diffusion phase change: application to the melting of a pure metal. Numer Heat Transf, Part A Appl 1988;13:297–318.
[6] Chamkha A, Doostanidezfuli A, Izadpanahi E, Ghalambaz M. Phase-change heat transfer of single/hybrid nanoparticles-enhanced phase-change materials over a heated horizontal cylinder confined in a square cavity. Adv Powder Technol 2016.
[7] Chamkha A, Ismael M, Kasaeipoor A, Armaghani T. Entropy generation and natural convection of CuO-water nanofluid in C-shaped cavity under magnetic field. Entropy 2016;18:50.
[8] Chandrasekar M, Suresh S, Bose AC. Experimental investigations and theoretical determination of thermal conductivity and viscosity of Al_2O_3/water nanofluid. Exp Thermal Fluid Sci 2010;34:210–16.
[9] Corcione M. Effects of the thermal boundary conditions at the sidewalls upon natural convection in rectangular enclosures heated from below and cooled from above. Int J Thermal Sci 2003;42:199–208.
[10] Duangthongsuk W, Wongwises S. Measurement of temperature-dependent thermal conductivity and viscosity of TiO_2-water nanofluids. Exp Thermal Fluid Sci 2009;33:706–14.
[11] Esfe MH, Afrand M, Yan W-M, Yarmand H, Toghraie D, Dahari M. Effects of temperature and concentration on rheological behavior of MWCNTs/SiO_2 (20–80)-SAE40 hybrid nano-lubricant. Int Commun Heat Mass Transf 2016;76:133–8.
[12] Esfe MH, Arani AAA, Rezaie M, Yan W-M, Karimipour A. Experimental determination of thermal conductivity and dynamic viscosity of Ag–MgO/water hybrid nanofluid. Int Commun Heat Mass Transf 2015;66:189–95.
[13] Esfe MH, Saedodin S, Mahmoodi M. Experimental studies on the convective heat transfer performance and thermophysical properties of MgO–water nanofluid under turbulent flow. Exp Thermal Fluid Sci 2014;52:68–78.
[14] Gau C, Viskanta R. Melting and solidification of a pure metal on a vertical wall. J Heat Transf 1986;108:174–81.
[15] Gharbi S, Harmand S, Jabrallah SB. Experimental comparison between different configurations of PCM based heat sinks for cooling electronic components. Appl Thermal Eng 2015;87:454–62.
[16] Harandi SS, Karimipour A, Afrand M, Akbari M, D'Orazio A. An experimental study on thermal conductivity of F-MWCNTs–Fe_3O_4/EG hybrid nanofluid: effects of temperature and concentration. Int Commun Heat Mass Transf 2016;76:171–7.
[17] Harikrishnan S, Kalaiselvam S. Preparation and thermal characteristics of CuO–oleic acid nanofluids as a phase change material. Thermochim Acta 2012;533:46–55.
[18] Heysiattalab S, Malvandi A, Ganji D. Anisotropic behavior of magnetic nanofluids (MNFs) at filmwise condensation over a vertical plate in presence of a uniform variable-directional magnetic field. J Mol Liq 2016;219:875–82.
[19] Ismael MA, Mansour M, Chamkha AJ, Rashad A. Mixed convection in a nanofluid filled-cavity with partial slip subjected to constant heat flux and inclined magnetic field. J Magn Magn Mater 2016;416:25–36.
[20] Jena P, Brocchi E, Motta M. *In-situ* formation of Cu–Al_2O_3 nano-scale composites by chemical routes and studies on their microstructures. Mater Sci Eng: A 2001;313:180–6.
[21] Jeong J, Li C, Kwon Y, Lee J, Kim SH, Yun R. Particle shape effect on the viscosity and thermal conductivity of ZnO nanofluids. Int J Refrig 2013;36:2233–41.
[22] Kashani S, Ranjbar A, Abdollahzadeh M, Sebti S. Solidification of nano-enhanced phase change material (NEPCM) in a wavy cavity. Heat Mass Transf 2012;48:1155–66.
[23] Khodadadi J, Hosseinizadeh S. Nanoparticle-enhanced phase change materials (NEPCM) with great potential for improved thermal energy storage. Int Commun Heat Mass Transf 2007;34:534–43.
[24] Khodadadi, J.M., 2015. Nanoparticle-enhanced phase change materials (NEPCM) with improved thermal energy storage. Google Patents.
[25] Kumar L, Manjunath B, Patel R, Markandeya S, Agrawal R, Agrawal A, et al. Experimental investigations on melting of lead in a cuboid with constant heat flux boundary condition using thermal neutron radiography. Int J Thermal Sci 2012;61:15–27.
[26] Ling Z, Zhang Z, Shi G, Fang X, Wang L, Gao X, et al. Review on thermal management systems using phase change materials for electronic components, Li-ion batteries and photovoltaic modules. Renew Sustain Energy Rev 2014;31:427–38.
[27] Liu Y-D, Zhou Y-G, Tong M-W, Zhou X-S. Experimental study of thermal conductivity and phase change performance of nanofluids PCMs. Microfluid Nanofluidics 2009;7:579–84.
[28] Madhesh D, Parameshwaran R, Kalaiselvam S. Experimental investigation on convective heat transfer and rheological characteristics of Cu–TiO_2 hybrid nanofluids. Exp Thermal Fluid Sci 2014;52:104–15.
[29] Makulati N, Kasaeipoor A, Rashidi M. Numerical study of natural convection of a water–alumina nanofluid in inclined C-shaped enclosures under the effect of magnetic field. Adv Powder Technol 2016;27:661–72.
[30] Malvandi A, Ganji D, Pop I. Laminar filmwise condensation of nanofluids over a vertical plate considering nanoparticles migration. Appl Thermal Eng 2016;100:979–86.
[31] Maruoka N, Akiyama T. Thermal stress analysis of PCM encapsulation for heat recovery of high temperature waste heat. J Chem Eng Jpn 2003;36:794–798.
[32] Maruoka N, Sato K, Yagi J-i, Akiyama T. Development of PCM for recovering high temperature waste heat and utilization for producing hydrogen by reforming reaction of methane. ISIJ Int 2002;42:215–19.
[33] Moghadassi A, Ghomi E, Parvizian F. A numerical study of water based Al_2O_3 and Al_2O_3–Cu hybrid nanofluid effect on forced convective heat transfer. Int J Thermal Sci 2015;92:50–7.
[34] Nabil M, Khodadadi J. Experimental determination of temperature-dependent thermal conductivity of solid eicosane-based nanostructure-enhanced phase change materials. Int J Heat Mass Transf 2013;67:301–10.
[35] Nomura T, Okinaka N, Akiyama T. Waste heat transportation system, using phase change material (PCM) from steelworks to chemical plant. Resour Conserv Recycl 2010;54:1000–6.
[36] Rashidi M, Ganesh NV, Hakeem AA, Ganga B, Lorenzini G. Influences of an effective Prandtl number model on nano boundary layer flow of γ Al_2O_3–H_2O and γ Al_2O_3–$C_2H_6O_2$ over a vertical stretching sheet. Intern J Heat Mass Transf 2016;98:616–23.
[37] Reddy JN. An introduction to the finite element method. New York: McGraw-Hill; 1993.
[38] Shalaby S, Bek M, El-Sebaii A. Solar dryers with PCM as energy storage medium: a review. Renew Sustain Energy Rev 2014;33:110–16.
[39] Sheremet MA, Oztop HF, Pop I, Abu-Hamdeh N. Analysis of entropy generation in natural convection of nanofluid inside a square cavity having hot solid block: Tiwari and Das' Model. Entropy 2015;18:9.
[40] Sheremet MA, Pop I, Shenoy A. Natural convection in a wavy open porous cavity filled with a nanofluid: Tiwari and Das' nanofluid model. Eur Phys J Plus 2016;131:1–12.
[41] Sundar LS, Singh MK, Sousa AC. Enhanced heat transfer and friction factor of MWCNT–Fe_3O_4/water hybrid nanofluids. Int Commun Heat Mass Transf 2014;52:73–83.
[42] Suresh S, Venkitaraj K, Selvakumar P, Chandrasekar M. Synthesis of Al_2O_3–Cu/water hybrid nanofluids using two step method and its thermo physical properties. Colloids Surf A: Physicochem Eng Asp 2011;388:41–8.
[43] Suresh S, Venkitaraj K, Selvakumar P, Chandrasekar M. Effect of Al_2O_3–Cu/water hybrid nanofluid in heat transfer. Exp Thermal Fluid Sci 2012;38:54–60.
[44] Tiari S, Qiu S, Mahdavi M. Numerical study of finned heat pipe-assisted thermal energy storage system with high temperature phase change material. Energy Convers Manag 2015;89:833–42.
[45] Tiari S, Qiu S, Mahdavi M. Discharging process of a finned heat pipe–assisted thermal energy storage system with high temperature phase change material. Energy Convers Manag 2016;118:426–37.
[46] Toghraie D, Chaharsoghi VA, Afrand M. Measurement of thermal conductivity of ZnO–TiO_2/EG hybrid nanofluid. J Thermal Anal Calorim 2016;125:527–35.
[47] Wu S, Zhu D, Zhang X, Huang J. Preparation and melting/freezing characteristics of Cu/paraffin nanofluid as phase-change material (PCM). Energy & fuels 2010;24:1894–8.
[48] Zaraki A, Ghalambaz M, Chamkha AJ, Ghalambaz M, De Rossi D. Theoretical analysis of natural convection boundary layer heat and mass transfer of nanofluids: Effects of size, shape and type of nanoparticles, type of base fluid and working temperature. Adv Powder Technol 2015;26:935–46.
[49] Zeng J, Sun L, Xu F, Tan Z, Zhang Z, Zhang J, et al. Study of a PCM based energy storage system containing Ag nanoparticles. J Therm Anal Calorim 2006;87:371–5.
[50] Zienkiewicz OC, Taylor RL, Nithiarasu P, 2013. The finite element method for fluid dynamics.